Applied Catalysis B: Environmental 164 (2015) 234–240

Contents lists available at ScienceDirect

Applied Catalysis B: Environmental

journal homepage: www.elsevier.com/locate/apcatb

Controllable sonochemical synthesis of $Cu_2O/Cu_2(OH)_3NO_3$ composites toward synergy of adsorption and photocatalysis

Songbo Wang[a], Xiangwen Zhang[a,b], Lun Pan[a,b], Feng-Min Zhao[a], Ji-Jun Zou[a,b,*], Tierui Zhang[c], Li Wang[a,b]

[a] Key Laboratory for Green Chemical Technology of the Ministry of Education, School of Chemical Engineering and Technology, Tianjin University, Tianjin 300072, China
[b] Collaborative Innovative Center of Chemical Science and Engineering (Tianjin), Tianjin 300072, China
[c] Key Laboratory of Photochemical Conversion and Optoelectronic Materials, Technical Institute of Physics and Chemistry, Chinese Academy of Sciences, Beijing 100190, China

ARTICLE INFO

Article history:
Received 18 January 2014
Received in revised form 22 August 2014
Accepted 15 September 2014
Available online 22 September 2014

Keywords:
Photocatalysis
Adsorption
Cuprous oxide
Copper hydroxide nitrate
Sonochemical synthesis

ABSTRACT

Composites having both maximized adsorption capability and high photocatalytic activity are very promising for pollutant removal by combining adsorption and photocatalysis. In this work, we report a facile sonochemical synthesis of Cu_2O(nanoparticles)/$Cu_2(OH)_3NO_3$(sheets) composites with tunable composition using only copper powders and $Cu(NO_3)_2$ as precursors. The composites can be controlled from almost pure Cu_2O (98.1%) to pure $Cu_2(OH)_3NO_3$ (95.9%) through adjusting the initial ratio of Cu^{2+}:Cu^0 and sonication time. Controlled experiments show that Cu_2O nanoparticles are formed first *via* the redox reaction between Cu^{2+} and Cu^0, after that Cu_2O are converted to $Cu_2(OH)_3NO_3$. $Cu_2(OH)_3NO_3$ synthesized using the sonochemical method exhibits outstanding adsorption capability toward organic dyes, subsequently Cu_2O can degrade them quickly *via* photocatalysis, so the $Cu_2O/Cu_2(OH)_3NO_3$ composites are very efficient to remove pollutant due to the synergetic effect of adsorption and photocatalysis. In particular, composite with 30.6% of $Cu_2(OH)_3NO_3$ and 69.4% of Cu_2O shows the highest removal capability and good stability.

© 2014 Elsevier B.V. All rights reserved.

1. Introduction

Cu_2O is p-type metal oxide semiconductor with a direct band gap of 2.0 eV and shows high photoactivity under visible light ($\lambda > 380$ nm), has been widely used in solar energy conversion, hydrogen evolution, and organic pollutants degradation in waste water [1–4]. Cu_2O nanoparticles have been synthesized by various methods, such as wet chemical reduction, electrodeposition, solvothermal synthesis and sonochemical synthesis. Huang et al. [5] synthesized Cu_2O nanocrystals in aqueous solution. Siegfried and Choi [6] investigated the morphological transformation of Cu_2O nanocrystals in electrochemical environment. Kumar et al. [7] synthesized amorphous Cu nanoparticles and nanocrystalline Cu_2O embedded in polyaniline matrices by sonochemical method. In most cases, reducing agents such as hydroxylamine ($NH_2OH{\cdot}HCl$) [8] and glutamic acid [9] are needed in the synthesis of Cu_2O. Recently, we developed a simple method to synthesize Cu_2O film *via* the redox reaction between Cu^{2+} ions and Cu foil in hydrothermal conditions, successfully controlled the morphology of the film by tuning the type of anions, and demonstrated the morphology-dependent photocatalytic performance and stability [10].

$Cu_2(OH)_3NO_3$, a basic Cu(II) salt with layered structure, has applications in vehicle airbags and ion exchangers [11]. It can also be employed as the precursor to prepare $Cu(OH)_2$ and CuO. Many approaches have been adopted to synthesize $Cu_2(OH)_3NO_3$, such as precipitation of $Cu(NO_3)_2$ in basic solution [12] and urea hydrolysis of $Cu(NO_3)_2$ [13]. The layered structure makes $Cu_2(OH)_3NO_3$ suitable for fabricating composite materials. Srikhaow and Smith [12] fabricated $Cu_2(OH)_3NO_3$/ZnO composites by one-step hydrothermally metal oxide assisted method.

Sonochemistry is a useful technique to produce materials with unusual properties and is now positioned as one powerful tool in nanostructured material synthesis [14,15]. The chemical effect

* Corresponding author at: Key Laboratory for Green Chemical Technology of the Ministry of Education, School of Chemical Engineering and Technology, Tianjin University, Tianjin 300072, China. Tel.: +86 22 27892340; fax: +86 22 27892340.
E-mail address: jj_zou@tju.edu.cn (J.-J. Zou).

http://dx.doi.org/10.1016/j.apcatb.2014.09.033
0926-3373/© 2014 Elsevier B.V. All rights reserved.

of ultrasound comes from acoustic cavitation (*i.e.*, the formation, growth, and implosive collapse of the bubbles in liquids) which produces unique hot spots that can achieve temperatures above 5000 K, pressures exceeding 1000 atm and heating and cooling rates in excess of 10^{10} Ks^{-1}, where free radicals such as $OH^{\bullet}$ and $H^{\bullet}$ will be generated by sonolysis of water [14,15]. These extreme conditions provide a unique means to drive chemical reactions.

Adsorption and photocatalysis are two fundamental ways for waste-water and gas treatment by removing pollutants like organic dyes [16–22]. Actually, surface adsorption is a prerequisite for photocatalysis [23,24], so the combination of adsorption and photocatalysis may lead to more efficient materials. Herein, we utilized ultrasound to replace the hydrothermal treatment to accelerate the redox reaction between Cu^{2+} and Cu^0, and synthesized Cu_2O particle at room temperature using only and $Cu(NO_3)_2$ and copper powder as the precursor. More importantly, we synthesized $Cu_2O/Cu_2(OH)_3NO_3$ composites with its composition varying from almost pure Cu_2O to pure $Cu_2(OH)_3NO_3$ by adjusting the Cu^{2+}:Cu^0 ratio and sonication time. $Cu_2(OH)_3NO_3$ prepared using the present method exhibits significant adsorption toward organic dyes, and the $Cu_2O/Cu_2(OH)_3NO_3$ composites are very efficient in the removal of dyes due to a synergetic effect of adsorption and photocatalysis.

2. Experimental

2.1. Materials

$Cu(NO_3)_2{\cdot}3H_2O$, $NaNO_3$, ethanol, 2-propanol and MO were all reagent grade and purchased from Tianjin Guangfu Fine Chemical Research Institute. Copper powders (99.9%, 50 nm) were purchased from Beijing Nachen Technology Development Co., Ltd, and their SEM image and XRD pattern are shown in Fig. S1 (Supporting Information, SI). Commercial Cu_2O (99.9%) was purchased from Alfa Aesar. Deionized water was used in all experiments. All the reagents were used as received.

2.2. Preparation of composites

In a typical synthesis, 0.2 g of copper powders and defined amount of $Cu(NO_3)_2{\cdot}3H_2O$ were mixed with 80 mL deionized water, then irradiated with a high-density ultrasonic horn (Ti-horn, 20 kHz, 50 W/cm^{-2}, Shanghai Bilon Instruments Co., Ltd.) at 35 °C with magnetic stirring for defined period. The suspension was centrifuged and the precipitates were washed with deionized water and ethanol for several times, and dried at 40 °C for 12 h. The materials were labeled as *S-R-t* according to molar ratio of Cu^{2+}:Cu (R) and sonication time (*t*, hour). For comparison, pure $Cu_2(OH)_3NO_3$ was synthesized according literature [11], 0.72 g $Cu(NO_3)_2{\cdot}3H_2O$ was added to 30 mL of 2-propanol under magnetic stirring at room-temperature, then the mixture was transferred into a Telfon-lined stainless steel autoclave and heated to 140 °C for 24 h. The product was washed with deionized water and ethanol for several times, and dried at 40 °C for 12 h.

2.3. Characterizations

XRD patterns were recorded using D/MAX-2500 X-ray diffractometer equipped with Cu Kα radiation at 40 kV and 140 mA at a scanning rate of 5°/min. SEM images were observed using a field-emission scanning electron microscope (FEI, Nanosem 430). HR-TEM observations were carried out using a Tecnai G^2 F-20 transmission electron microscope with a field-emission gun operating at 200 kV. Selected-area electron diffraction (SAED) patterns were obtained from JEM-100CX II electron microscope (JEOL). FT-IR spectra were obtained on a Bruker Vertex-70 FT-IR spectrometer. TG analysis was conducted on a TGA Q500 thermogravimeter under N_2 flow at a rate of 5 °C/min. X-ray photoelectron spectrum (XPS) analysis was conducted with a PHI-1600 X-ray photoelectron spectroscope equipped with Al Kα radiation, and the binding energy was calibrated by the C1s peak (284.6 eV) of the contamination carbon. Specific surface area (S_{BET}) was calculated based on N_2 adsorption/desorption isotherms conducted on Micromeritics Tri-Star 3000 at 77 K, all samples were outgassed under vacuum at 100 °C for 4 h. The zeta potential (ζ-potential) was measured in suspension (0.2 g L^{-1}, 25 °C, pH = 6.0) using Zeta Nanosizer (ZEN 3600, Malvern Ltd.).

2.4. Adsorption and photodegradation

Adsorption of organic dyes (methyl orange, MO) was conducted in an opening quartz chamber (150 mL) in dark. 20 mg of $Cu_2O/Cu_2(OH)_3NO_3$ composites and 1 mL of MO (6 mmol L^{-1}) were dispersed in 100 mL of deionized water. Then the suspension was stirred until MO was totally adsorbed. During this test, 1.5 mL of liquid was taken out at intervals, centrifuged and the concentration of MO in the filtrate was analyzed using Hitachi U-3010 UV–vis spectrometer at wavelength of 463 nm). 1 mL of MO (6 mmol L^{-1}) solution was added again, which was repeated several times till adsorption saturation. In addition, deionized water was added to compensate the volume loss by sampling.

After adsorption saturation, photodegradation was conducted in the same chamber at ambient conditions (25 °C) under irradiation using a 300 W high pressure Xe lamp (CEL-HXUV 300, Beijing Aulight Co., Ltd.) with a UV cutoff filter (λ > 400 nm). Once MO was completely degraded as determined by UV–vis spectrometer, 1 mL of MO (6 mmol L^{-1}) was added again, which was repeated several times in 400 min.

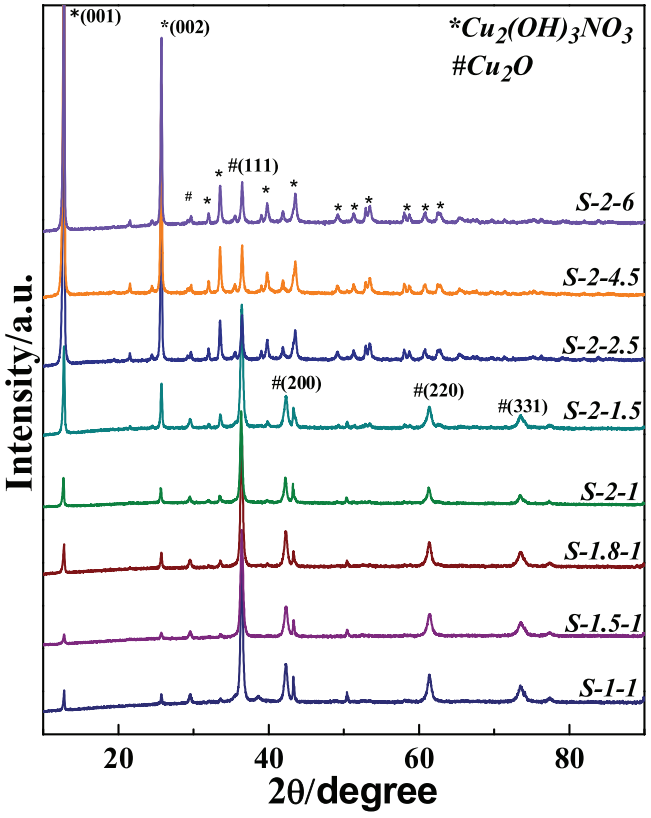

Fig. 1. XRD patterns of $Cu_2O/Cu_2(OH)_3NO_3$ composites.

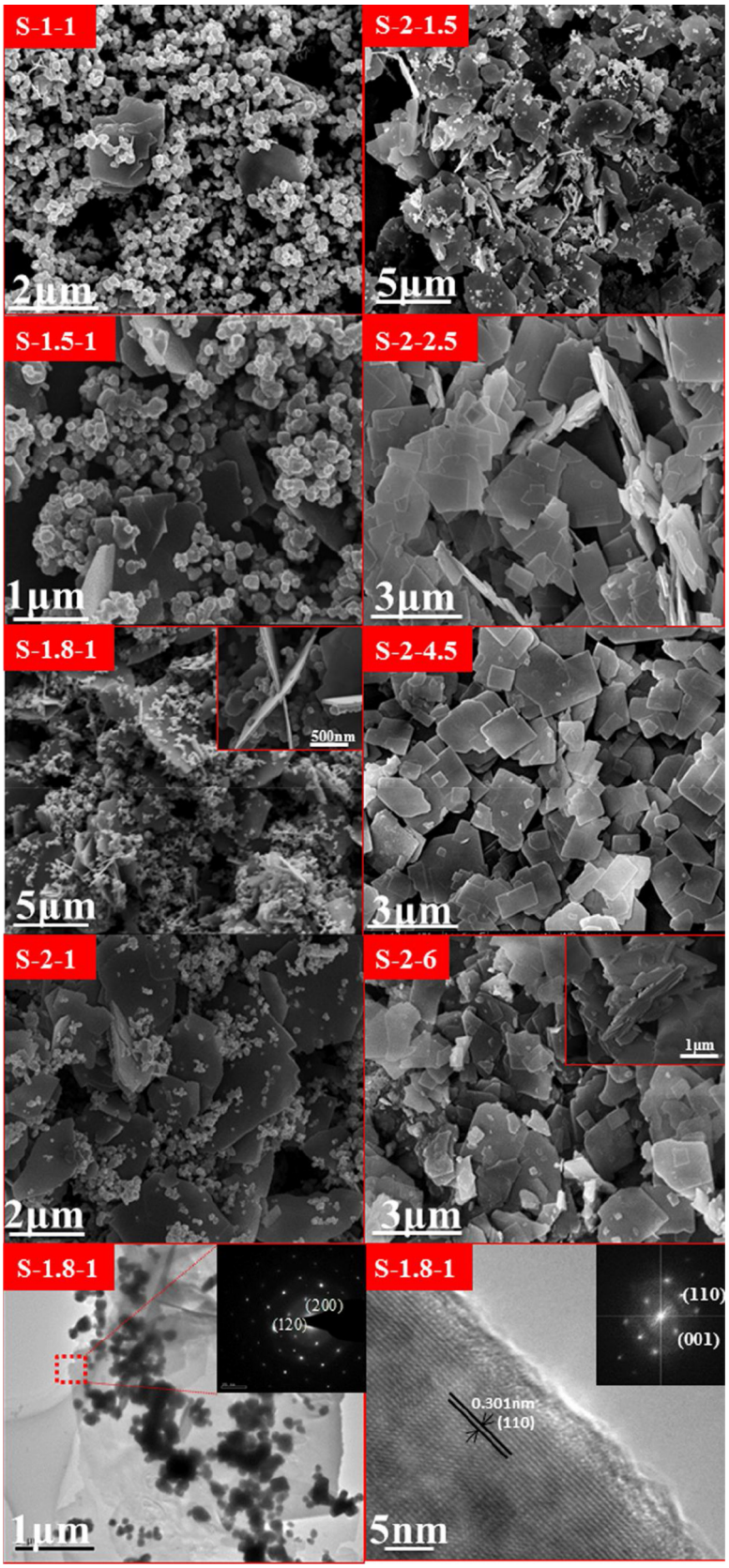

Fig. 2. SEM and TEM images of $Cu_2O/Cu_2(OH)_3NO_3$ composites. Insets in S-1.8-1 and S-2-6 are vertical view of the sheet; insets in TEM images of S-1.8-1 are SAED patterns of the particles and the sheet.

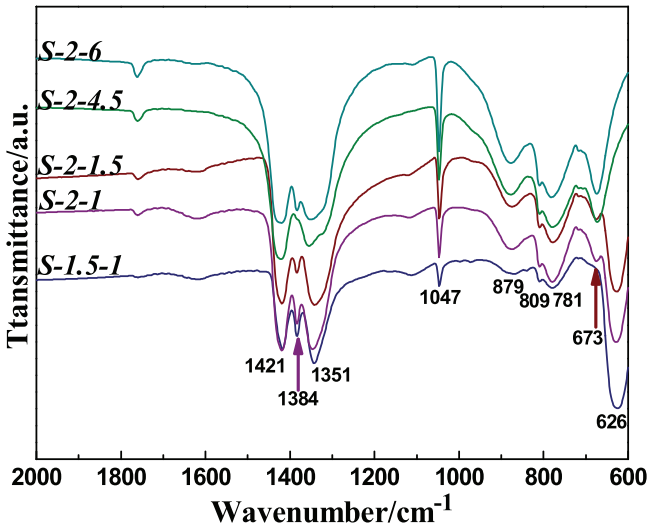

Fig. 3. FT-IR spectra of $Cu_2O/Cu_2(OH)_3NO_3$ composites.

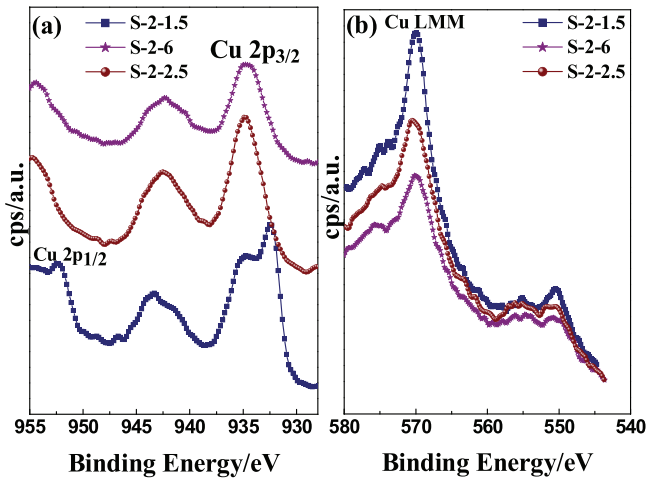

Fig. 4. Cu2p XPS spectra and Cu LMM auger transition spectra of $Cu_2O/Cu_2(OH)_3NO_3$ composites.

3. Results and discussion

3.1. Structure and morphology of composites

XRD patterns (Fig. 1) show the materials obtained under ultrasound irradiation are composites of cubic Cu_2O (JCPDS No. 78-2076) and monoclinic $Cu_2(OH)_3NO_3$ (JCPDS No. 75-1779), although their composition varies in a wide range from nearly pure Cu_2O to pure $Cu_2(OH)_3NO_3$. No diffraction peaks of either CuO or $Cu(OH)_2$ phases were observed. SEM images (Fig. 2) show that the composites are composed of many nanoparticles about 100 nm and sheets about 5 μm. High resolution TEM image shows the lattice space of nanoparticles is 0.301 nm which corresponds to the distance of (1 1 1) planes of cubic Cu_2O [5]. SAED patterns also show the (1 1 0) and (0 0 1) facets of Cu_2O. As for the sheet, the well aligned SAED spots reveal a simple monoclinic structure, and the major spots are indexed to (1 2 0) and (2 0 0) facets of $Cu_2(OH)_3NO_3$. Thus, the nanoparticles and sheets observed in SEM are Cu_2O and $Cu_2(OH)_3NO_3$, respectively.

FT-IR spectra (Fig. 3) also confirm the formation of $Cu_2(OH)_3NO_3$ and Cu_2O in the composites. The peaks at 879 cm^{-1}, 781 cm^{-1} and 673 cm^{-1} can be indexed to the hydrogen bonding frequencies related to Cu—O—H of $Cu_2(OH)_3NO_3$ [12,13]. The presence of NO_3^- is evidenced by the vibration bands from middle to lower wavenumbers: 1421 cm^{-1}, 1384 cm^{-1}, 1351 cm^{-1} (ν_3),1047 cm^{-1} (ν_1) and 809 cm^{-1} (ν_2) [11]. It is noted that, the signals of Cu—O—H in S-2-6 are much stronger than those in S-1.5-1, meanwhile S-1.5-1 shows a strong peak at 626 cm^{-1} which is related to characteristic peak of Cu_2O [25–27]. Therefore, S-2-6 contains more $Cu_2(OH)_3NO_3$ while S-1.5-1 has more Cu_2O, in agreement with the XRD patterns in Fig. 1.

Fig. 4 presents the XPS spectra of typical samples. For S-2-2.5 and S-2-6, the peak around 934.4 eV assigned to $Cu2p_{3/2}$ indicates the presence of Cu^{2+} [25,28–30]. The extra shake-up satellite peak at 942.4 eV implying the presence of unfilled Cu $3d^9$ shell further confirms the existence of Cu^{2+} in the composites [10,28]. However, for S-2-1.5, these peaks are broadened, suggesting the existence of Cu in other chemical states. In particular, a more strong $Cu2p_{3/2}$ peak appears at 932.3 eV which is referred to Cu^0 or Cu^+ [29–32], and the LMM transition indicates the peak is consistent with Cu^+ (569.9 eV) instead of Cu^0 (568 eV) [33]. This again suggests that the amount of Cu_2O and $Cu_2(OH)_3NO_3$ in the composites are variable.

3.2. Tunable content of composites

To determine the content of Cu_2O and $Cu_2(OH)_3NO_3$ qualitatively, the composites were analyzed by TG. As shown in Fig. 5, the weight loss below 150 °C is due to the loss of physically adsorbed water, whereas the weight loss at temperature of 190–250 °C is caused by the decomposition of $Cu_2(OH)_3NO_3$ following the mechanism described in Eq. (1) [11,13].

$$Cu_2(OH)_3NO_3 \rightarrow 2CuO + HNO_3\,(g) + H_2O\,(g) \quad (1)$$

We also measured the TG profile of pure Cu_2O and $Cu_2(OH)_3NO_3$, the weight loss of Cu_2O is negligible (0.3%), while the weight loss of $Cu_2(OH)_3NO_3$ is 33.8%, which is identical to the theoretical weight loss of pure $Cu_2(OH)_3NO_3$ (33.6%), so the content of $Cu_2(OH)_3NO_3$ in each sample can be calculated on the bases of weight loss from 190 °C to 250 °C. Additionally, the content of Cu_2O and $Cu_2(OH)_3NO_3$ is also calculated according to the area of Cu_2O (1 1 1) and $Cu_2(OH)_3NO_3$ (0 0 1) XRD peak. To do this, physical mixtures of Cu_2O and $Cu_2(OH)_3NO_3$ with known composition were used as reference. As included in Table 1, the composites range from almost pure Cu_2O (98.1%) to pure $Cu_2(OH)_3NO_3$ (95.9%), and the data determined using the two methods are very close. Besides, we noted slightly weight increasing above 300 °C in Fig. 5a. This increase is also observed in other Cu_2O-containing materials [34], probably due to the reaction of Cu_2O with N_2 or trace amount of oxygen in N_2 flow.

It is found that varying the ratio of Cu^{2+}:Cu^0 in the starting materials can lead to dramatically change in the composition of composites. With sonication time of 1 h, when the ratio of Cu^{2+}:Cu^0 increases from 1:1 to 2:1, the (0 0 1) peak of $Cu_2(OH)_3NO_3$ become stronger, see the XRD patterns in Fig. 1. SEM images in Fig. 2 also show that the $Cu_2(OH)_3NO_3$ sheets gradually grow at the expense

Table 1
Content of $Cu_2(OH)_3NO_3$ in $Cu_2O/Cu_2(OH)_3NO_3$ composites.

Samples	$Cu_2(OH)_3NO_3$/%[a]	Samples	$Cu_2(OH)_3NO_3$/%
S-1-1	1.9	S-2-1	24.1(24.6)
S-1-1.5	7.4	S-2-1.5	30.7(27.8)
S-1-7.5	92.4	S-2-2	62.6
S-1.5-1	8.2(8.7)	S-2-2.5	92.1(93.1)
S-1.8-1	13.9	S-2-4.5	94.1(94.4)
S-1.8-2.5	37.0	S-2-6	95.9

[a] Mass content, the data in bracket are based on XRD result and others are based on TG.

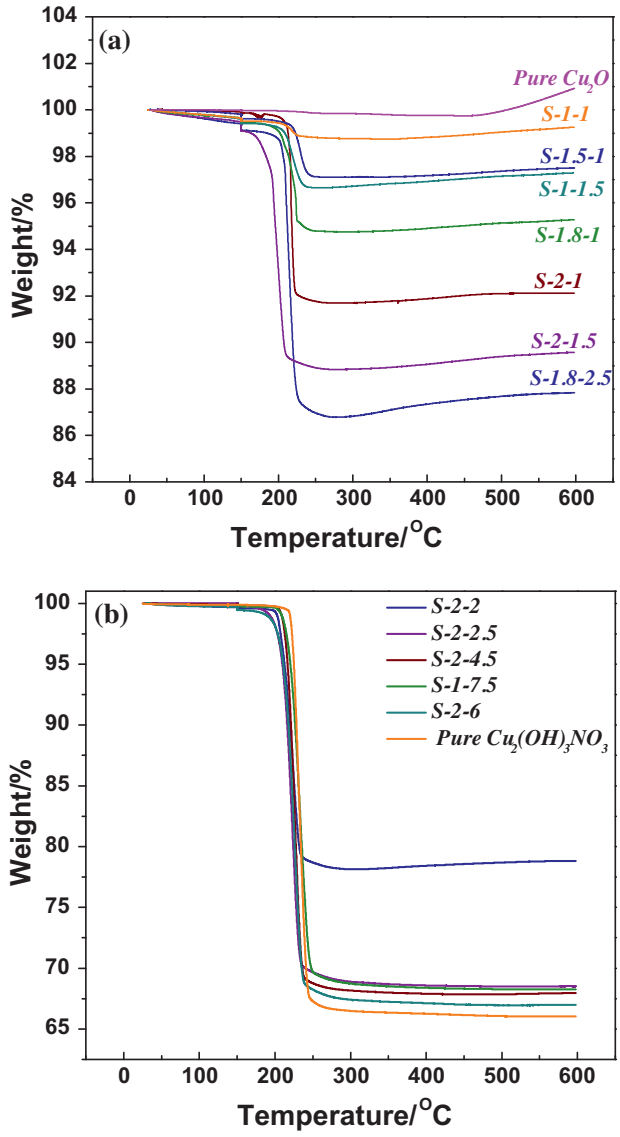

Fig. 5. TG profile of $Cu_2O/Cu_2(OH)_3NO_3$ composites.

of Cu_2O nanoparticles. Actually, from Table 1, one can see a clear rise in the content of $Cu_2(OH)_3NO_3$ from 1.9% (S-1-1) to 24.1% (S-2-1).

Also, prolonging the sonication time can increase the content of $Cu_2(OH)_3NO_3$ rapidly. In the case of Cu^{2+}:Cu^0 ratio = 2, when the sonication time is less than 2.5 h, Cu_2O is the major component (~69%). After sonication for 4.5 h, Cu_2O nanoparticles disappear and only $Cu_2(OH)_3NO_3$ sheets are visible in SEM images (Fig. 2), with the content of $Cu_2(OH)_3NO_3$ reaching 94.1%. Accordingly, the (0 0 1) peak of $Cu_2(OH)_3NO_3$ overwhelms the (1 1 1) peak of Cu_2O (Fig. 1). At lower Cu^{2+}:Cu^0 ratio, long sonication time also promotes the content of $Cu_2(OH)_3NO_3$, see S-1.8-2.5 and S-1.8-1 in Table 1. In particular, S-1-7.5 (Fig. S2, SI) has 92.4% $Cu_2(OH)_3NO_3$ while S-1-1 contains only 1.96% $Cu_2(OH)_3NO_3$.

3.3. Formation mechanism of composites

It has been reported that $Cu_2(OH)_3NO_3$ can be formed under weakly acid conditions with the presence of NO_3^- [2,35]. Since $OH^\bullet$ radicals are easy to generate under ultrasound irradiation [14], $Cu_2(OH)_3NO_3$ may be formed from Cu^{2+}, NO_3^- and hydrolyzed $OH^\bullet$. However, when $Cu(NO_3)_2$ solution is sonicated alone for 9 h, no $Cu_2(OH)_3NO_3$ precipitates are formed, suggesting that $Cu_2(OH)_3NO_3$ is not formed in this way. Furthermore, we sonicated Cu powders in water for 6 h but did not get any $Cu_2(OH)_3NO_3$ or Cu_2O, so Cu cannot be converted to Cu_2O or $Cu_2(OH)_3NO_3$ without the presence of $Cu(NO_3)_2$ under ultrasound irradiation.

As shown in Table 1, from S-2-1 to S-2-1.5, the increase in the content of $Cu_2(OH)_3NO_3$ is very limited. From S-2-1.5 to S-2-2.5, however, the formation of $Cu_2(OH)_3NO_3$ is proportional to the sonication time. This suggests that Cu_2O is formed at the beginning and then $Cu_2(OH)_3NO_3$ is derived from Cu_2O. It can be seen in Fig. 2 that the $Cu_2(OH)_3NO_3$ sheets grow with the prolonging of sonication time, corresponding to the disappearance of Cu_2O particles, which also hints the transformation of Cu_2O to $Cu_2(OH)_3NO_3$.

In order to understand the formation mechanism of $Cu_2O/Cu_2(OH)_3NO_3$ composites, a controlled experiment was conducted. First, $Cu(NO_3)_2$ and Cu with molar ratio of 1:1 were sonicated for 1.5 h, and a composite with $Cu_2(OH)_3NO_3$ of 7.4% was obtained (labeled as *S-c-1.5*, the color is brick-red). Then 0.5376 g $NaNO_3$ was added into the suspension to make the Cu: NO_3^- molar ratio reaches 1:2. After sonication for another 3 h (labeled as *S-c-4.5*), the color of the suspension becomes light green, and the content of $Cu_2(OH)_3NO_3$ in the composite reaches 94.6%. XRD and SEM characterizations (Fig. S3, SI) also show that Cu_2O is formed at the first stage and then $Cu_2(OH)_3NO_3$ is generated at the expense of Cu_2O. This confirms that $Cu_2(OH)_3NO_3$ is formed *via* the reaction between NO_3^- and Cu_2O. In addition, we found that when $Cu(NO_3)_2$ and Cu with molar ratio of 2:1 (S-2) is stirred for very long time (more than 14 h) without ultrasound, the solution also become light green which indicates the formation of $Cu_2(OH)_3NO_3$. Thus ultrasound irradiation can accelerate the formation of $Cu_2(OH)_3NO_3$ significantly.

Now we are able to explain how the $Cu_2O/Cu_2(OH)_3NO_3$ composites are formed, see Scheme 1. As reported in our previous work, Cu_2O can be formed *via* the redox reaction between Cu^{2+} and Cu^0 [10]. This reaction is quite slow under ambient conditions but accelerated considerably under ultrasound irradiation (Eq. (2)). Accordingly, the pH value of the suspension is decreased, for example, from 3.7 to 2.8 after 1 h sonication for Cu^{2+}:Cu^0 at ratio of 2:1. Then Cu_2O is converted to $Cu_2(OH)_3NO_3$ with NO_3^-, H^+, and $OH^\bullet$ radicals comes from water (Eqs. (3) and (4)). Obviously, long sonication time or high concentration of NO_3^- can enhance the reaction and thus increase the content of $Cu_2(OH)_3NO_3$.

$$Cu^{2+} + Cu + H_2O \xrightarrow{))))} Cu_2O + 2H^+ \quad (2)$$

$$H_2 \xrightarrow{))))} H^\bullet + OH^\bullet \quad (3)$$

$$Cu_2O + 2OH^\bullet + NO_3^- + H^+ \xrightarrow{))))} Cu_2(OH)_3NO_3 \quad (4)$$

3.4. Removal of dyes using composites

It is well known that Cu_2O can be used as photocatalyst to remove organic pollutants *via* photodegradation. To demonstrate the potential application of $Cu_2O/Cu_2(OH)_3NO_3$ composites, the samples were utilized to eliminate MO (a widely used probe molecule to evaluate the visible-light-induced photocatalytic activity of Cu_2O [5,36–38]) by combining adsorption in dark and then photocatalysis under visible light. Both adsorption and photocatalysis were conducted for many cycles to evaluate the maximum capability, as shown in Fig. S4 (SI), according to which the saturation adsorption and photodegradation capability were calculated and shown in Fig. 6.

First we focus on the adsorption capacity of the composites. The composites majorly containing $Cu_2(OH)_3NO_3$ show very fast adsorption rate and strong adsorption capacity. For example, S-2-6 (containing 95.9% of $Cu_2(OH)_3NO_3$) can adsorb almost all the

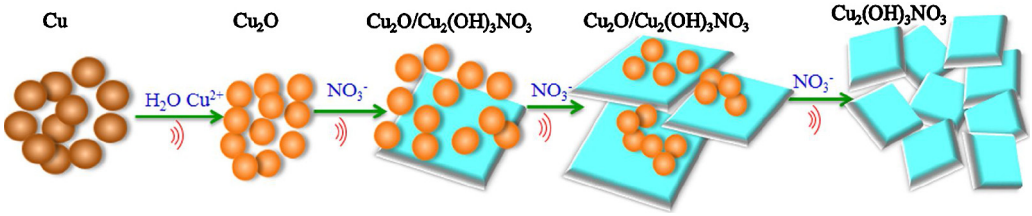

Scheme 1. Schematic illustration of the formation of $Cu_2O/Cu_2(OH)_3NO_3$ composites.

MO within 7 min in the first round and the cycle can run four times within 100 min, with the saturation adsorption as high as 1.62 mmol MO g^{-1}. However, the adsorption capability declines with the decrease of $Cu_2(OH)_3NO_3$ in the composites. For S-1-1 (containing 1.9% of $Cu_2(OH)_3NO_3$), with Cu_2O as the main component, the first round adsorption cannot be finished in 200 min and the adsorption on this material is negligible. Therefore, the strong adsorption of S-2-6 must be attributed to the presence of $Cu_2(OH)_3NO_3$.

Very recently, it is reported that $Cu_2(OH)_3NO_3$/ZnO composite can remove MO *via* catalytic wet oxidation with the presence of oxygen [12]. To determine whether this reaction happens in the present work, one experiment was conducted under continuous nitrogen bubbling to exclude the oxygen in the solution. As shown in Fig. 6 and Fig. S5 (SI), the same amount of MO can still be removed, which clearly proves that the decolorization of MO in dark is due to adsorption. Moreover, the composites were recovered after the adsorption and analyzed by XRD, FT-IR, and XPS. As shown in Fig. 7, new peaks at 17.2°, 25.1° and 45.3° corresponding to MO absorbed on the materials appear in the XRD patterns. And all the characteristic bands of MO can be found in the FT-IR spectra (Fig. 8). Moreover, N1s XPS signal located at 399.3 eV is shifted about 7.5 eV compared with the case before adsorption (Fig. S6, SI), which can be assigned to C—N bond in MO. These results confirm that the removal of MO in dark is attributed to adsorption instead of oxidation.

We also prepared pure $Cu_2(OH)_3NO_3$ according to literature [11]. However, the adsorption ability (0.65 mmol MO g^{-1}, Fig. S7, SI) is just 40.1% of the sample synthesized in the present work, which suggests that $Cu_2(OH)_3NO_3$ fabricated using the present ultrasound method is excellent adsorbent. It should be noted that the BET surface area of the composites is lower (4.53 and 9.32 m^2/g for S-2-1.5 and S-2-4.5, respectively) than that of pure $Cu_2(OH)_3NO_3$ (15.4 m^2/g), but the adsorption capability is better than the latter one. As shown in Table 2, the ζ-potential data (measured at pH = 6.0 that is identical to the adsorption experiments) indicates

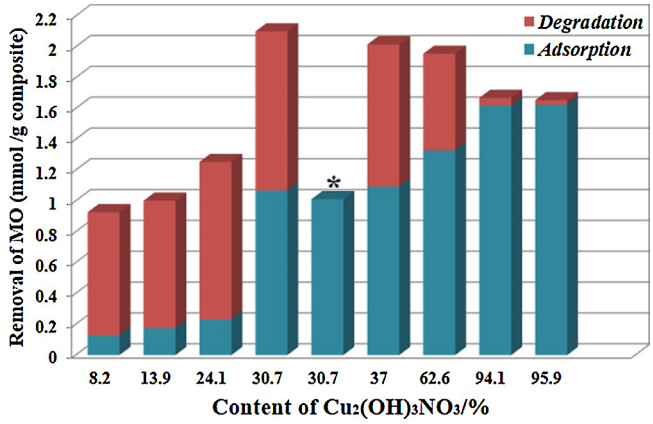

Fig. 6. Amount of MO removed by adsorption and photodegradation using $Cu_2O/Cu_2(OH)_3NO_3$ composites. The column with asterisk is the adsorption in N_2 atmosphere.

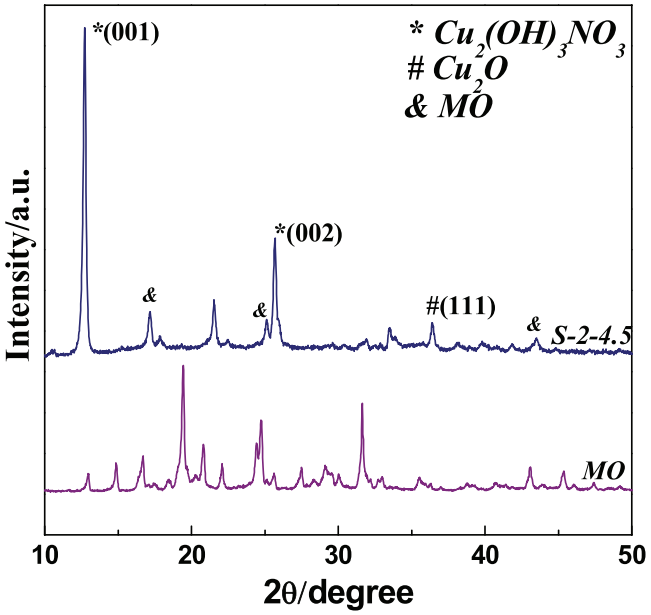

Fig. 7. XRD patterns of $Cu_2O/Cu_2(OH)_3NO_3$ composites after adsorption of MO.

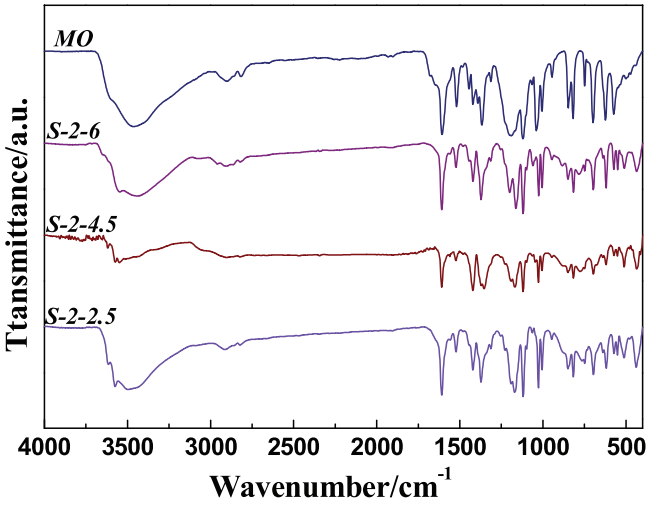

Fig. 8. FT-IR spectra of $Cu_2O/Cu_2(OH)_3NO_3$ composites after adsorption of MO.

that the composites are positively charged, which favors adsorption of negatively charged MO [23,39]. In addition, it is noted that the ζ-potential increases with $Cu_2(OH)_3NO_3$ content, indicative of increasing adsorption capability.

Table 2
Zeta potentials of $Cu_2O/Cu_2(OH)_3NO_3$ composites.

Sample	S-1-1	S-2-1.5	S-2-2	S-2-6
Zeta potential/mV	39.2	41.3	43.3	53.1

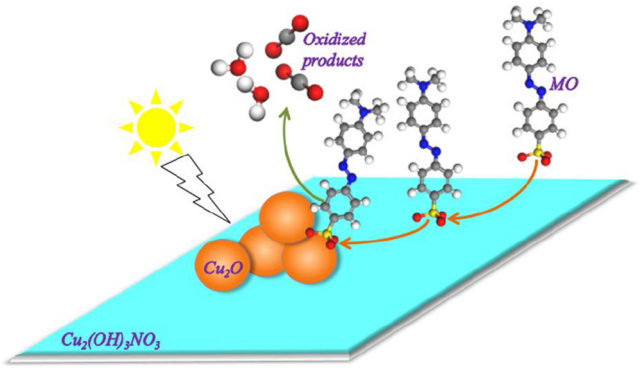

Scheme 2. Synergetic effect of adsorption and photocatalysis over $Cu_2O/Cu_2(OH)_3NO_3$ composites.

Contrary to the adsorption, no report proves $Cu_2(OH)_3NO_3$ is photoactive, so the photodegradation is dependent on the content of Cu_2O. The self-decomposition (Fig. S8, SI) and dye-sensitization of MO under visible light is negligible [23,40,41], whereas Cu_2O can act as good photocatalyst to degrade MO under visible light [5,8,36–38]. As shown in Fig. 6, the samples with more Cu_2O show better photocatalytic performance. Nevertheless, the composites mainly containing $Cu_2(OH)_3NO_3$ (S-2-4.5 and S-2-6) show ignorable photoactivity, for which the first degradation run cannot be completed even in more than 200 min.

Importantly, regarding to the overall removal ability *via* adsorption and photocatalysis, a balance has to be made to get the highest efficiency. The composite (S-2-1.5) with 30.6% of $Cu_2(OH)_3NO_3$ and 69.4% of Cu_2O is the most capable of removing MO. This phenomenon shows the synergetic advantage of adsorption and photoreaction, as illustrated in Scheme 2. In the composites, Cu_2O nanoparticles are dispersed on the $Cu_2(OH)_3NO_3$ sheet. The strong adsorption capability of $Cu_2(OH)_3NO_3$ sheet can enrich MO from the solution by chemical adsorption. Then the adsorbed MO molecules move on the sheet, reach Cu_2O surface and are degraded. So a suitable composition that can balance the adsorption and photoreaction shows the highest efficiency. In addition, the composites also show good photostability after the adsorption and photocatalysis, as indicated by the unchanged XRD patterns of used composites (Fig. S9, SI).

4. Conclusions

We developed a simple sonochemical method to synthesize Cu_2O (nanoparticles)/$Cu_2(OH)_3NO_3$ (sheets) composites using copper powders and $Cu(NO_3)_2$ as precursor. The composition can be tuned from almost pure Cu_2O (98.1%) to pure $Cu_2(OH)_3NO_3$ (95.9%) according to the ratio of Cu^{2+}:Cu^0 in the starting materials and the sonication time. Cu_2O is formed firstly and then transferred to $Cu_2(OH)_3NO_3$ under ultrasound irradiation. $Cu_2(OH)_3NO_3$ is excellent adsorbent for organic dyes, and Cu_2O is good photocatalyst for MO degradation. As a result, $Cu_2O/Cu_2(OH)_3NO_3$ composites are very efficient for the removal of MO due to the synergetic effect of adsorption and photocatalysis, and the composite consisting 30.6% of $Cu_2(OH)_3NO_3$ and 69.4% of Cu_2O is the most efficient.

Acknowledgment

The authors appreciate the supports from the National Natural Science Foundation of China (21222607), the Program for New Century Excellent Talents in Universities (NCET-09-0594), and the Foundation of Key Laboratory of Photochemical Conversion and Optoelectronic Materials, TIPC, Chinese Academy of Sciences (PCOM201302).

Appendix A. Supplementary data

Supplementary material related to this article can be found, in the online version, at http://dx.doi.org/10.1016/j.apcatb.2014.09.033.

References

[1] A. Paracchino, V. Laporte, K. Sivula, M. Grätzel, E. Thimsen, Nat. Mater. 10 (2011) 456–461.
[2] M. Yin, C.K. Wu, Y. Lou, C. Burda, J.T. Koberstein, Y. Zhu, S. O'Brien, J. Am. Chem. Soc. 127 (2005) 9506–9511.
[3] H. Shi, K. Yu, F. Sun, Z. Zhu, CrystEngComm 14 (2012) 278–285.
[4] L. Wu, L.K. Tsui, N. Swami, G. Zangari, J. Phys. Chem. C 114 (2010) 11551–11556.
[5] W.C. Huang, L.M. Lyu, Y.C. Yang, M.H. Huang, J. Am. Chem. Soc. 134 (2012) 1261–1267.
[6] M.J. Siegfried, K.S. Choi, Angew. Chem. Int. Ed. 117 (2005) 3282–3287.
[7] R.V. Kumar, Y. Mastai, Y. Diamant, A. Gedanken, J. Mater. Chem. 11 (2001) 1209–1213.
[8] J.Y. Ho, M.H. Huang, J. Phys. Chem. C 113 (2009) 14159–14164.
[9] H. Zhang, Q. Zhu, Y. Zhang, Y. Wang, L. Zhao, B. Yu, Adv. Funct. Mater. 17 (2007) 2766–2771.
[10] L. Pan, J.-J. Zou, T.R. Zhang, S. Wang, Z. Li, L. Wang, X. Zhang, J. Phys. Chem. C 118 (2014) 16335–16343.
[11] B. Liu, Nanoscale 4 (2012) 7194–7198.
[12] A. Srikhaow, S.M. Smith, Appl. Catal. B 130–131 (2013) 84–92.
[13] C. Henrist, K. Traina, C. Hubert, G. Toussaint, A. Rulmont, R. Cloots, J. Cryst. Growth 254 (2003) 176–187.
[14] J.H. Bang, K.S. Suslick, Adv. Mater. 22 (2010) 1039–1059.
[15] H. Xu, B.W. Zeiger, K.S. Suslick, Chem. Soc. Rev. 42 (2013) 2555–2567.
[16] Q. Xiang, K. Lv, J. Yu, Appl. Catal. B 96 (2010) 557–564.
[17] L. Pan, J.-J. Zou, S. Wang, X.Y. Liu, X. Zhang, L. Wang, ACS Appl. Mater. Interfaces 4 (2012) 1650–1655.
[18] L. Pan, J.-J. Zou, S. Wang, Z.-F. Huang, A. Yu, L. Wang, X. Zhang, Chem. Commun. 49 (2013) 6593–6595.
[19] A. Houas, H. Lachheb, M. Ksibi, E. Elaloui, C. Guillard, J.-M. Herrmann, Appl. Catal. B 31 (2001) 145–157.
[20] Z.-F. Huang, J.-J. Zou, L. Pan, S. Wang, X. Zhang, L. Wang, Appl. Catal. B 147 (2014) 167–174.
[21] D. Mohan, C.U. Pittman Jr., J. Hazard. Mater. 142 (2007) 1–53.
[22] J.-J. Zou, Y. Liu, L. Pan, L. Wang, X. Zhang, Appl. Catal. B 95 (2010) 439–445.
[23] L. Pan, J.-J. Zou, X. Zhang, L. Wang, J. Am. Soc. Chem. 133 (2011) 10000–10002.
[24] L. Pan, J.-J. Zou, S. Wang, Z.F. Huang, X. Zhang, L. Wang, Appl. Surf. Sci. 268 (2013) 252–258.
[25] A. Ahmed, N.S. Gajbhiye, A.G. Joshi, J. Solid State Chem. 184 (2011) 2209–2214.
[26] W. Sun, W. Sun, Y. Zhuo, Y. Chu, J. Solid State Chem. 184 (2011) 1638–1643.
[27] H.M. Yang, J. Ouyang, A.D. Tang, Y. Xiao, X.W. Li, X.D. Dong, Y.M. Yu, Mater. Res. Bull. 41 (2006) 1310–1318.
[28] Z. Zhang, P. Wang, J. Mater. Chem. 22 (2012) 2456–2464.
[29] V.V. Nikesh, A.B. Mandale, K.R. Patil, S. Mahamuni, Mater. Res. Bull. 40 (2005) 694–700.
[30] W.Z. Wang, G.H. Wang, X.S. Wang, Y.J. Zhan, Y.K. Liu, C.L. Zheng, Adv. Mater. 14 (2002) 67–69.
[31] M. Yang, J. Xu, J. Wei, J.-L. Sun, W. Liu, J.L. Zhu, Appl. Phys. Lett. 100 (2012) 253113.
[32] I.L. Soroka, A. Shchukarev, M. Jonsson, N.V. Tarakina, P.A. Korzhavyi, Dalton Trans. 42 (2013) 9585–9594.
[33] T. Ghodselahi, M.A. Vesaghi, A. Shafiekhani, A. Baghizadeh, M. Lameii, Appl. Surf. Sci. 255 (2008) 2730–2734.
[34] C.Y. Kim, T. Sekino, K. Niihara, Mater. Res. Innov. 5 (2002) 201–207.
[35] K. Chen, D. Xue, CrystEngComm 14 (2012) 8068–8075.
[36] Y. Sui, Y. Zeng, L. Fu, W. Zheng, D. Li, B. Liu, B. Zou, RSC Adv. 3 (2013) 18651–18660.
[37] H. Yu, J. Yu, S. Liu, S. Mann, Chem. Mater. 19 (2007) 4327–4334.
[38] L. Huang, F. Peng, H. Yu, H. Wang, Solid State Sci. 11 (2009) 129–138.
[39] C. Hu, Y. Wang, H. Tang, Appl. Catal. B 30 (2001) 277–285.
[40] B. Tian, J. Zhang, T. Tong, F. Chen, Appl. Catal. B 79 (2008) 394–401.
[41] X. Yan, T. Ohno, K. Nishijima, R. Abe, B. Ohtani, Chem. Phys. Lett. 429 (2006) 606–610.